Precision Measurements and Computations of Transition Energies in Rotationally Cold Triatomic Hydrogen Ions up to the Midvisible Spectral Range

Michele Pavanello,[1,*] Ludwik Adamowicz,[1] Alexander Alijah,[2] Nikolai F. Zobov,[3] Irina I. Mizus,[3] Oleg L. Polyansky,[3] Jonathan Tennyson,[4] Tamás Szidarovszky,[5] Attila G. Császár,[5] Max Berg,[6] Annemieke Petrignani,[6,†] and Andreas Wolf[6]

[1]*Department of Chemistry and Biochemistry, The University of Arizona, Tucson, Arizona 85721, USA*
[2]*GSMA, UMR CNRS 7731, Université de Reims Champagne-Ardenne, U.F.R. Sciences Exactes et Naturelles, 51687 Reims Cedex 2, France*
[3]*Institute of Applied Physics, Russian Academy of Science, Ulyanov Street 46, Nizhnii Novgorod, Russia 603950*
[4]*Department of Physics and Astronomy, University College London, London WC1E 6BT, United Kingdom*
[5]*Laboratory of Molecular Spectroscopy, Institute of Chemistry, Eötvös University, H-1518 Budapest 112, P.O. Box 32, Hungary*
[6]*Max-Planck-Institut für Kernphysik, D-69117 Heidelberg, Germany*

(Received 29 August 2011; published 11 January 2012)

First-principles computations and experimental measurements of transition energies are carried out for vibrational overtone lines of the triatomic hydrogen ion H_3^+ corresponding to floppy vibrations high above the barrier to linearity. Action spectroscopy is improved to detect extremely weak visible-light spectral lines on cold trapped H_3^+ ions. A highly accurate potential surface is obtained from variational calculations using explicitly correlated Gaussian wave function expansions. After nonadiabatic corrections, the floppy H_3^+ vibrational spectrum is reproduced at the 0.1 cm^{-1} level up to 16 600 cm^{-1}.

DOI: 10.1103/PhysRevLett.108.023002 PACS numbers: 33.20.−t, 31.15.A−, 31.50.Bc, 37.10.Ty

In quantitative understanding of small molecules, a door to extreme precision was opened for H_2 through Herzberg's measurements [1] and the theoretical work of Kolos and Wolniewicz [2], which led to a complete reproduction and assignment of the spectrum. Subsequently, analogous efforts shifted to the smallest triatomic molecular system, the H_3^+ ion. The complexity of this system greatly increases as its vibrations become floppy already by infrared excitation at about 10 000 cm^{-1}, roughly a third of its dissociation energy. Hence, even after 35 years of activity and despite enormous advances in computers and experimental methods, the H_3^+ spectrum at higher excitations has remained an enigma neither fully accessed experimentally nor fully elucidated theoretically. For example, the intriguing, near-dissociation spectrum of H_3^+ reported by Carrington *et al.* [3,4] is still unassigned and poorly understood almost 30 years after it was recorded.

In theoretical molecular physics, H_3^+ has always been a benchmark polyatomic for high-level electronic-structure computations. They started with the pioneering works of Hirschfelder [5], who explained the stability of the ion and then, after Coulson [6] first hypothesized on its structure, Christoffersen [7] brought in theoretical numerical evidence showing the equilibrium structure to be an equilateral triangle some 14 years before this was demonstrated experimentally. H_3^+ has also been a test case for multidimensional nuclear-motion calculations starting with the work of Carney and Porter [8].

Close interplay between theory and experiments characterized the spectroscopy of H_3^+ and was fundamental in probing its rotational-vibrational (ro-vib) infrared spectrum. *Ab initio* calculations were vital for the first laboratory observation of the H_3^+ infrared spectrum [9] and the first astronomical detection of H_3^+ in the ionosphere of Jupiter [10]. However, the H_3^+ ro-vib spectrum in the visible region has remained unseizable for both theory and experiments. Once the barrier to linearity at ∼10 000 cm^{-1} is exceeded on the ground-state electronic potential energy surface (PES), the vibrations become floppy and sample vast regions of the PES at barely restricted geometries. As experiments advance beyond this barrier, they struggle with the strong decrease of all spectral intensities (lower by about a factor of 10^6 compared to the fundamental transition [11]) while past first-principles predictions became increasingly inaccurate and lost their ability to guide experimental line searches and spectral identifications [12]. This roadblock persisted despite recent theoretical advances [11,13–17], in which increasingly more accurate and complete H_3^+ PESs have been determined.

In this work we report developments that decisively change this situation and largely unveil the elusive, highly excited H_3^+ spectrum. Experimentally, we present advances in the sensitivity of ion trap spectroscopy on H_3^+ allowing us to measure the frequencies of ro-vib transitions extending far into the visible spectral range. Theoretically, we develop a model which reproduces these observations and is capable of describing the full ro-vib spectrum of H_3^+.

The quantum-mechanical treatment of molecules usually starts with relativistic effects excluded and, in principle, could proceed by an all-particle, direct solution of the nonrelativistic Schrödinger equation. This methodology has been proven successful for many diatomics [18]. However, for H_3^+ such a direct approach involves 12 degrees of freedom, presenting serious technical problems

presently unresolved. Hence, even for this five-body system, we are forced to initially make the Born-Oppenheimer (BO) approximation, which splits the H_3^+ Schrödinger equation into an electronic equation (solved for relevant, fixed arrangements of the nuclei) and a nuclear one describing the ro-vib motion. The energies generated in the electronic equation create the PES upon which the nuclei move. The solutions of the nuclear Schrödinger equation provide energies (and corresponding wave functions) representing different ro-vib states of the system. Beyond BO corrections are introduced. The diagonal adiabatic (DA) correction accounts to first order for the neglected coupling between the motions of the nuclei and the electrons. Further terms included are the nonadiabatic (NA) corrections and, on a smaller scale, those accounting for relativistic (REL) effects. QED corrections and corrections due to the finite size of the proton are of even smaller size, and are not included here. While the latter corrections are certainly much smaller than the accuracy of the present calculations, the magnitude of the former for the transitions lying near the barrier to linearity, estimated based on the calculations of the QED α^3 and α^4 corrections for H_2 [19] and HD [20], is about -0.07 cm^{-1}, i.e., of similar magnitude as the present accuracy. The neglect of QED effects constitutes the largest source of error in our calculations. (The determination of these effects will be carried out in our future work.)

The theoretical innovation, which has been key to the present work, is the development of a very efficient method for solving the electronic Schrödinger equation. The approach is variational and employs explicitly correlated shifted Gaussian (ECSG) basis functions to expand the electronic wave function of the system. ECSGs [21,22] are the following functions of the coordinates of all the electrons of the molecule:

$$g_k(\mathbf{r}) = \exp[(\mathbf{r} - \mathbf{s}_k)' \bar{\mathbf{A}}_k (\mathbf{r} - \mathbf{s}_k)]. \quad (1)$$

The vectors $\mathbf{r}$ and $\mathbf{s}_k$ are $3n$ dimensional and represent the Cartesian coordinates of the electrons and of the Gaussian shifts (for a two-electron system $n = 2$), respectively, and the prime denotes vector transposition. Contrary to mainstream orbital-based electronic-structure methods, here the Gaussian shifts (also referred to as ''Gaussian centers'') are not restricted to the nuclear positions. $\bar{\mathbf{A}}_k$ is a $3n \times 3n$ symmetric matrix collecting the Gaussian exponential parameters. In the variational calculation, the energy of the system is minimized by optimizing the $\bar{\mathbf{A}}_k$ and $\mathbf{s}_k$ parameters of each ECSG function in the set. What sets our method apart from other ECSG implementations [13,14] is the use of analytic energy gradients determined with respect to ECSG parameters during the minimization [18,22].

The computations of ro-vib energies involve four steps. In the first step, we employ 900 ECSGs in the electronic wave function expansion to calculate the BO energies and DA correction for 42 498 nuclear geometries of the H_3^+ ion. This is by far the most complete and dense grid of points used to determine the H_3^+ PES. The energy at each nuclear geometry is significantly more accurate than in any previous calculation [13,14]. We estimate that at each PES point our energy is consistently ~ 0.1 cm^{-1} above the exact nonrelativistic BO energy [22]. The work took 9 months of continuous calculations on a 210-CPU parallel computer system. In the second step, the energy points are fitted with a global, analytic function. The fitting function is a sum of polynomials of the H_3^+ vibrational modes expressed in symmetry coordinates (i.e., no mass scaling) and consists of two separate terms, one in the form of a diatomics-in-molecules function [23], representing asymptotic regions of the PES near and above dissociation, and a short-range three-body term [24] representing the region where all three nuclei are located closer to each other and interact more strongly. 297 terms are included in the fitting function, which are composed by polynomials of order up to 15, to ensure high accuracy of the fit in all areas of the PES. The rms of the fit is 0.097 cm^{-1}—an unprecedented low value, representing a 2 orders of magnitude improvement over previous attempts. Up to energies of 20 000 cm^{-1}, the maximum deviation is only 0.19 cm^{-1}. In the third step, the PES is augmented with surfaces accounting for the DA and the relativistic corrections. The DA corrections were determined at each PES point with the Born-Handy method [25], while the relativistic corrections to the electronic BO energies were taken from Ref. [14] and fitted separately (rms of 0.007 cm^{-1} and maximum deviation of 0.02 cm^{-1} for both the DA and REL surfaces). Finally, the fourth step involves solving the triatomic nuclear-motion Schrödinger equation using the DVR3D suite of programs [17]. In this step, the ro-vib NA effects are accounted for with the mass-scaling method of Polyansky and Tennyson [17], in which the vibrational masses of the protons are made heavier than the nuclear masses by about $0.4753 m_e$ [26].

In the measurements, we apply spectroscopy by chemical probing [27,28] using mass-separated product ion counting at a cryogenic rf multipole trap. The very high sensitivity of this method was demonstrated recently [28] for H_3^+ lines up to 13 300 cm^{-1}. Modifications detailed below allowed us to observe even weaker lines up to 16 600 cm^{-1} and to access the H_3^+ spectrum far beyond the 13 700 cm^{-1} limit of the most recent discharge-cell measurements [12].

As in previous work [28], H_3^+ ions from a rf storage source are injected into the cryogenic trap filled with He ($\sim 2 \times 10^{14}$ cm^{-3}), Ar ($\sim 1 \times 10^{12}$ cm^{-3}), and H_2 ($\sim 2 \times 10^{10}$ cm^{-3}) and cooled to a temperature of 60 K. A 200 ms long precooling ensures that most of the H_3^+ ions descend to the two lowest rotational levels ($J = 1$) of the vibrational ground state. Light from a single-mode Ti:sapphire or a dye laser was then applied along the trap

axis for 100 ms, completing a 300-ms storage cycle. The detection of laser transitions exploits the reaction $H_3^+ + Ar \rightarrow ArH^+ + H_2$, which is endothermic but activated by ro-vib excitation of H_3^+ above $\sim$4500 cm^{-1}. Ions released from the trap are mass filtered and counted, switching between detection of ArH^+ (signal) and H_3^+ (normalization) from one storage cycle to the next. The scheme was adapted to trap and count much higher numbers of H_3^+ ions than before. For this, an ion guiding system was added between the ion source and the trap, improving their vacuum separation and allowing the H_2 pressure in the source to be set independently of the gas densities in the trap. Moreover, pulse stretching was implemented when releasing the trapped ions, ensuring linear counting of the trap inventory up to several 10^4 H_3^+ ions (a factor of 25 higher than previously). Finally, fourfold retroreflection of the laser path through the trap increased the effective laser power by a factor of $\sim$2 and stable operation times were increased up to days. Typically, a few hundred storage cycles were required at each laser frequency for a laser excitation signal to become detectable. The wavelength scans were controlled by a wave meter that was regularly calibrated by a laser source stabilized on the D_2 line of ^{6}Li ($2^2S_{1/2} \rightarrow 2^2P_{3/2}$) at 14 903.633(1) cm^{-1} [29] through Doppler-free spectroscopy.

Unobserved lines from previous theoretical predictions by Neale *et al.* (NMT) [11] and Schiffels *et al.* (SAH03) [16] were searched in scans at $\sim$0.01 cm^{-1} steps, combining contiguous ranges of $\sim$0.3 cm^{-1} and covering 1 cm^{-1} in $\sim$6 h. Fine scans over located lines used $\sim$0.003 cm^{-1} steps; Gaussian profiles were then fitted to obtain the line centers with a calibration-limited precision of $\pm$0.005 cm^{-1}. Because only the two lowest rotational levels of H_3^+ are sufficiently populated, predicted observable lines are typically separated by more than 20 cm^{-1}. As the experiment was performed before the present calculations were completed, the previous predictions guided the line searches in this work. The inaccuracy of those predictions, particularly at higher wave numbers, led to long search times. We should note that for the infrared lines the present rf trap method yields perfect agreement [26] with the discharge spectroscopy method [12].

The newly observed lines, all but one in the visible spectral region, are detailed in Table I together with their upper-level quantum numbers and the differences to present and previous theoretical predictions (exp $-$calc). The measured lines have very low intensity. For example, the Einstein B coefficient of the 15 450.112(5) cm^{-1} line was estimated by Neale *et al.* [11] to be $B = 7.7 \times 10^{17}$ cm^3 J^{-1} s^{-2}. This is almost 10^6 times lower than that of the 2529.724(5) cm^{-1} line of the fundamental transition [28] with intensity $B = 4.77 \times 10^{23}$ cm^3 J^{-1} s^{-2}. In addition, it is about a factor of 3 lower than the weakest among the calculated strengths for the transitions measured by Kreckel *et al.* [28] (2.03×10^{18} cm^3 J^{-1} s^{-2}). The energetic match with the calculated lines unambiguously defines the upper-level J and the nuclear symmetry of the observed transitions. The assignment of quantum numbers v_1, v_2, ℓ, and G (these numbers are increasingly less representative of the quantum states as the excitation level increases) for some of the calculated high-lying states was taken from previous works [16,31] and confirmed by

TABLE I. Experimental (exp) high overtone transition frequencies for rotationally cold H_3^+ ions from the 00^0 vibrational ground state. Estimated experimental errors (dominated by wave number calibration) are in parentheses. The exp $-$calc are the deviations between the experimental and calculated (calc) transitions determined with respect to the calculated line positions best matching the experimental lines. The calculated results from earlier *ab initio* predictions (NMT [11] and SAH03 [16]) and the present work, using the BO PES (BO column), the PES that includes the DA corrections (+ DA column), the BO + DA predictions corrected for NA effects using the Polyansky and Tennyson model [17] (+ NA column), and the predictions with the BO + DA + REL PES also corrected for the NA effects (+ REL column). Quantum numbers specified [30] as (J, G) for lower-level (i) and upper-level (f) rotation and by $v_1 v_2^{|\ell|}$ for upper-level vibration. For the upper levels, only J and the nuclear symmetry (*para* and *ortho* for lower-level $G = 1$ and 0, respectively) are precise, and additional assignments have been taken from Refs. [16,26,31].

			exp $-$calc (cm^{-1})					
						This work		
$(J, G)_i$	$v_1 v_2^{\|\ell\|}(J, G)_f$	exp (cm^{-1}) (This work)	NMT	SAH03	BO	+DA	+NA	+REL
(1, 1)	07^1 (0, 1)	13 638.251(5)	1.65	0.49	3.54	−1.29	−0.18	−0.22
(1, 1)	08^2 (0, 2)	15 058.680(5)	0.49	1.13	2.14	−1.22	0.22	0.15
(1, 1)	16^2 (1, 2)	15 130.480(5)	0.44	1.70	1.03	−1.34	0.09	0.03
(1, 0)	16^2 (2, 3)	15 450.112(5)	−3.41	0.47	−1.48	−1.54	0.02	−0.06
(1, 0)	16^4 (2, 3)	15 643.052(5)	−0.76	1.91	−0.29	−1.44	0.12	0.04
(1, 1)	25^1 (1, 1)	15 716.813(5)	−2.25	0.91	1.08	−1.35	0.24	0.16
(1, 0)	34^2 (2, 3)	16 506.139(5)	(− 0.67)[a]	3.31	0.49	−1.38	0.33	0.23
(1, 1)	$J = 1$[b]	16 660.240(5)	(− 8.14)[a]	3.40	−0.50	−1.53	0.09	0.02

[a]Predicted nearby level of different J, guiding the experimental line search.
[b]Further assignment not available.

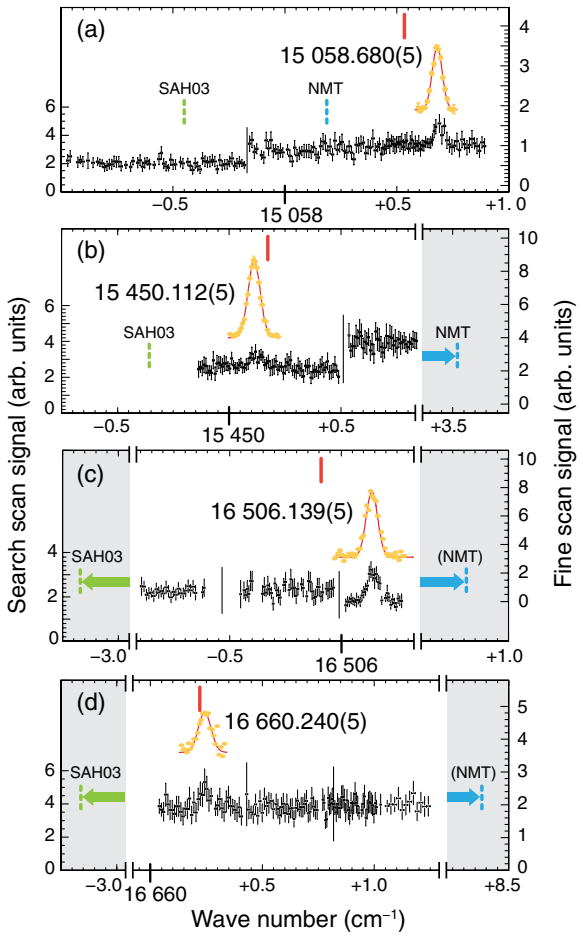

FIG. 1 (color online). Visible-light spectroscopy of cold trapped H_3^+ ions for some of the measured lines detailed in Table I. Top marks (full lines): present theoretical results. Orange (gray) symbols and fitted curves: fine scans (right-hand vertical scales) with Doppler-broadened line profiles (effective ion temperature ~85 K). Dashed marks: earlier predictions by NMT [11] and SAH03 [16] as labeled (arrows and shading indicate scale offsets). Black symbols: search scans (see the text) with breaks marked by thin vertical lines (left-hand vertical scales).

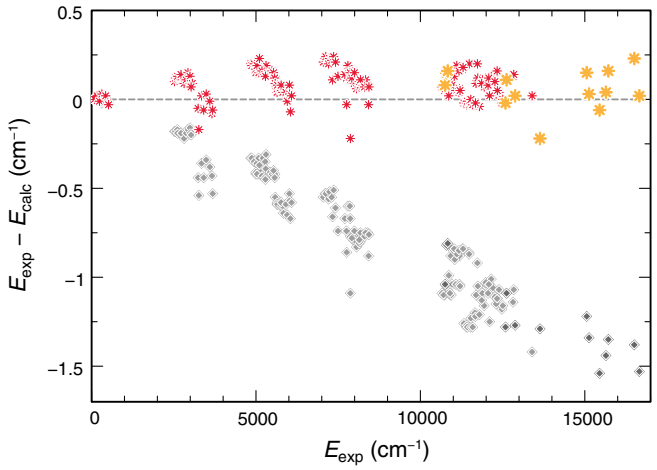

FIG. 2 (color online). Differences between experimental transition energies E_{exp} and the present calculation (E_{calc}) for the BO + DA PES (diamonds) and for the BO + DA + REL PES plus NA corrections (asterisks). Small red asterisks and light gray diamonds: using experimental data from Refs. [12,28,30,32] ($J \leq 3$ initial levels); large orange asterisks and dark gray diamonds: present data with 00^0 (1, 0) and (1, 1) initial levels.

additional analysis [26]. Search scans, fine scans, and theoretical line centers are shown for some cases in Fig. 1. The positions of the visible spectral lines are very well reproduced by the most complete model (+ REL) of the present computations. Instead of exp −calc differences of up to 3 cm^{-1} or even more displayed by the previous calculations, the deviations are now significantly reduced with a remaining rms deviation determined with respect to the measured data being only ~0.1 cm^{-1}. This represents more than an order of magnitude improvement over previous *ab initio* computations and also a significant improvement over semiempirical models [31] of the spectrum. In Fig. 2 we show the exp −calc differences for the present theory in the entire 0–16 600 cm^{-1} spectral region and for $J \leq 3$ initial levels. Employing the BO + DA surface in the nuclear calculations produces ro-vib energies whose deviations from the experiment systematically increase from a very small number for the lowest transitions to about −1.5 cm^{-1} for the highest ones. However, when the results are corrected for the REL and NA effects, excellent agreement with the experiments is reached. The vibrational wave functions [26] of the investigated states on the calculated PES show large probability density near linear configurations of the nuclei, thus demonstrating the significant role of such geometries in the investigated energy region.

In conclusion, this work provides the most accurate global ground-state H_3^+ PES available to date. Together with a simple model for nonadiabatic effects, it has allowed us to predict the ro-vib transitions of H_3^+ with unprecedented accuracy. By measurements extending far into the visible region, our calculations are shown to match the observed spectral lines with an average deviation as low as 0.1 cm^{-1}. The high predictive power of the present theory and the extreme experimental sensitivity achieved open the door to further measurements of the H_3^+ spectrum at even higher energies. Moreover, the accuracy of the present global PES and its large spatial extent set the foundation for describing and assigning the transitions in the Carrington spectrum [3,4] which stretches into the dissociative continuum. The near-dissociation region of the H_3^+ PES is also important for understanding proton collisions with hydrogen molecules. Finally, we note that PES calculations with ECSGs, although computationally expensive, are not restricted to two-electron systems; they could thus form a new paradigm for near-experimental-accuracy

ab initio predictions of spectra also for other few-electron molecular systems.

This work is supported by the Max Planck Society, the Russian Fund for Basic Research, the Scientific Research Fund of Hungary (Grant OTKA K72885), the European Union, and the European Social Fund (Grant Agreement No. TÁMOP 4.2.1/B-09/1/KMR-2010-0003). M. P. is supported by a Marie Curie Fellowship of the European Commission (PIIF-GA-2009-254444).

*Current address: Leiden Institute of Chemistry, Leiden University, PO Box 9502, 2300 RA Leiden, The Netherlands.
m.pavanello@chem.leidenuniv.nl

†Current address: Leiden Observatory, Leiden University, PO Box 9513, 2300 RA Leiden, The Netherlands.

[1] G. Herzberg, Science **177**, 123 (1972).
[2] W. Kolos and L. Wolniewicz, J. Mol. Spectrosc. **54**, 303 (1975).
[3] A. Carrington, J. Buttenshaw, and R. A. Kennedy, Mol. Phys. **45**, 753 (1982).
[4] A. Carrington, I. R. McNab, and Y. D. West, J. Chem. Phys. **98**, 1073 (1993).
[5] J. O. Hirschfelder, J. Chem. Phys. **6**, 795 (1938).
[6] C. A. Coulson, Proc. Cambridge Philos. Soc. **31**, 244 (1935).
[7] R. E. Christoffersen, J. Chem. Phys. **41**, 960 (1964).
[8] G. D. Carney and R. N. Porter, J. Chem. Phys. **60**, 4251 (1974).
[9] T. Oka, Phys. Rev. Lett. **45**, 531 (1980).
[10] P. Drossart *et al.*, Nature (London) **340**, 539 (1989).
[11] L. Neale, S. Miller, and J. Tennyson, Astrophys. J. **464**, 516 (1996).
[12] C. P. Morong, J. L. Gottfried, and T. Oka, J. Mol. Spectrosc. **255**, 13 (2009).
[13] W. Cencek, J. Rychlewski, R. Jaquet, and W. Kutzelnigg, J. Chem. Phys. **108**, 2831 (1998).
[14] R. A. Bachorz, W. Cencek, R. Jaquet, and J. Komasa, J. Chem. Phys. **131**, 024105 (2009).
[15] R. Jaquet, Theor. Chem. Acc. **127**, 157 (2010).
[16] P. Schiffels, A. Alijah, and J. Hinze, Mol. Phys. **101**, 189 (2003).
[17] O. L. Polyansky and J. Tennyson, J. Chem. Phys. **110**, 5056 (1999).
[18] S. Bubin, M. Cafiero, and L. Adamowicz, Adv. Chem. Phys. **131**, 377 (2005).
[19] K. Piszczatowski, G. Lach, M. Przybytek, J. Komasa, K. Pachucki, and B. Jeziorski, J. Chem. Theory Comput. **5**, 3039 (2009).
[20] K. Pachucki and K. Komasa, Phys. Chem. Chem. Phys. **12**, 9188 (2010).
[21] J. Rychlewski, in *Progress in Theoretical Chemistry and Physics*, edited by J. Maruani and S. Wilson (Kluwer Academic, Dordrecht, 2003), Vol. 13.
[22] M. Pavanello and L. Adamowicz, J. Chem. Phys. **130**, 034104 (2009).
[23] F. O. Ellison, J. Am. Chem. Soc. **85**, 3540 (1963).
[24] L. P. Viegas, A. Alijah, and A. J. C. Varandas, J. Chem. Phys. **126**, 074309 (2007).
[25] W. Cencek and W. Kutzelnigg, Chem. Phys. Lett. **266**, 383 (1997).
[26] See Supplemental Material at http://link.aps.org/supplemental/10.1103/PhysRevLett.108.023002 for additional documentation regarding (a) the inclusion of non-adiabatic effects, (b) the experimental setup and calibration, (c) vibrational assignment, and (d) plots of selected vibrational wave functions.
[27] S. Schlemmer, T. Kuhn, E. Lescop, and D. Gerlich, Int. J. Mass Spectrom. **185–187**, 589 (1999).
[28] H. Kreckel, D. Bing, S. Reinhardt, A. Petrignani, M. Berg, and A. Wolf, J. Chem. Phys. **129**, 164312 (2008).
[29] W. Scherf, O. Khait, H. Jäger, and L. Windholz, Z. Phys. D **36**, 31 (1996).
[30] C. Lindsay and B. J. McCall, J. Mol. Spectrosc. **210**, 60 (2001).
[31] A. Alijah, J. Mol. Spectrosc. **264**, 111 (2010).
[32] J. L. Gottfried, B. J. McCall, and T. Oka, J. Chem. Phys. **118**, 10890 (2003).